dc-electric-field-induced second-harmonic generation in Si(111)-SiO_2-Cr metal-oxide-semiconductor structures

O. A. Aktsipetrov,* A. A. Fedyanin, E. D. Mishina, and A. N. Rubtsov
Department of Physics, Moscow State University, Moscow 119899, Russia

C. W. van Hasselt, M. A. C. Devillers, and Th. Rasing
Research Institute for Materials, University of Nijmegen, Toernooiveld 1, NL 6525 Ed Nijmegen, The Netherlands

(Received 1 December 1995)

The mechanism of dc-electric-field-induced second-harmonic generation (EISH) was studied at the buried Si(111)-SiO_2 interface in transmission through a planar Si-SiO_2-Cr MOS structure. The second-harmonic contribution of the field-induced quadratic polarization generated in the space-charge region is determined. The role of the spatial distribution of the dc electric field inside the silicon space-charge region is demonstrated, as well as the influence of the oxide thickness. We have developed a phenomenological model of the EISH taking into account the interference between field-dependent and field-independent contributions to the nonlinear polarization (nonlinear interference) as well as the retardation of the EISH wave. We show that, due to these interference effects, the minima of the EISH curves do not coincide with the flatband voltage. [S0163-1829(96)07627-8]

I. INTRODUCTION

The silicon-silicon-oxide-buried interface has been a topic of intensive studies due to its key role in semiconductor technology. Important issues are to identify interfacial imperfections, such as point defects, charge traps, and dislocations; to understand their origin; and to develop *in situ* techniques to characterize the interface. Optical second-harmonic generation (SHG) is a sensitive tool for studying the characteristics of buried solid-electrolyte and solid-solid interfaces, as has been demonstrated in a number of experiments.[1–3] The SHG technique was shown to be extremely sensitive to the structural symmetry,[4–6] and steps and kinks on (vicinal) surfaces,[7–9] as well as to electronic transitions[10,11] and interfacial roughness.[5,12,13] Here we show that SHG is a very sensitive probe of the charge distribution near the Si(111)-SiO_2 interface.

dc-electric-field-induced SHG (EISH) at a Si(111)-SiO_2-electrolyte interface was discovered by Lee, Chang, and Bloembergen.[14] Since 1984 this phenomenon has been studied intensively, and a simple phenomenological model of EISH was developed for the Si-SiO_2-electrolyte interface.[15–17] This model predicted a quadratic dependence of the SHG intensity on the bias voltage, taking into account the effects of surface states and carrier degeneracy as well as the influence of the silicon oxide layer. Deviations from a parabolic bias dependence were already observed, that were attributed to carrier degeneracy[17] and to mobile charges.[18] In a more realistic approach to EISH the nonlinear interference of dc-induced and field-independent contributions to the nonlinear polarization as well as retardation effects in the nonlinear response should be taken into account. The latter cannot be ignored for several reasons. First, the width of the space-charge region (SCR) in silicon, where the EISH signal is generated, is comparable with the second-harmonic wavelength in Si. Thus the EISH wave undergoes a significant phase shift that changes the total SHG intensity. Second, the SCR width depends on the applied voltage. Therefore, one cannot simply take into account the retardation of the EISH response as a dressing of the cubic nonlinear susceptibility, as can be done for the bulk quadrupole contribution. Although the electrochemical technique allows us to apply significant dc electric fields at the semiconductor surface, the region of field values is restricted by electrochemical oxidation processes that occur at the silicon surface at anodic potentials. Therefore, the investigation of the EISH in metal-oxide-semiconductor (MOS) structures, that was demonstrated in Ref. 18 and recently extended to the planar MOS structures with semitransparent gate electrodes,[19,20] seems very promising.

The principal objectives of this paper are the investigation of the electric-field-induced SHG in transmission of IR fundamental light through Si(111)-SiO_2-Cr MOS structures for varying oxide thicknesses, and the development of a more correct phenomenological model of EISH at the Si-SiO_2 interface. Strong parabolic dependences of the SHG intensity on the applied bias with ascillatoriclike features are observed for a wide region of oxide thicknesses. The minimum of the parabolic dependence in the SHG intensity is shown to be shifted with respect to the flatband potential as obtained from capacitance-voltage (C-V) measurements. These shifts and the oscillatoric fine structure of the bias dependences can be explained successfully with a simple nonlinear optical model that properly takes into account the nonlinear interference and retardation effects. The influence of the spatial distribution of the dc electric field inside the SCR on EISH is demonstrated. We show that the oxide-thickness dependence of the SHG response from the Si-SiO_2 interface can be described by taking into account multiple reflections in the oxide film and the distribution of the bias voltage across the MOS structure due to the voltage drop over the SiO_2 layer. The influence of charges, trapped at the Si-SiO_2 interface, on the SHG intensity is discussed.

II. ELECTRIC-FIELD-INDUCED SHG

SHG is symmetry forbidden in the bulk of cubic centrosymmetric crystals within electric dipole approximation,

 © 1996 The American Physical Society

TABLE I. Nonzero components of the nonlinear tensor susceptibility $\chi^{(3)}(2\omega;\omega,\omega,0,)$ produced the dc-induced nonlinear polarization $\mathbf{P}^{\rm BD}$, for the Si crystal, calculated in the crystallographic frame XYZ. The latter is chosen in such a way that $X\|\langle 100\rangle$, $Y\|\langle 010\rangle$, and $Z\|\langle 001\rangle$ crystallographic directions.

	χ_1	χ_2	χ_3
$\chi_{\alpha\beta\gamma\delta}$	$XXXX=YYYY=$ $=ZZZZ$	$XYXY=XYYX=$ $=YYXX=YXYX=$ $=XXZZ=XZXZ=$ $=YYZZ=YZYZ$	$XYYX=YXXY=$ $=XZZX=YZZY=$ $=ZXXZ=ZYYZ$

and the SHG response arises from the surface electric dipole and bulk electric quadrupole contributions to the nonlinear polarization given by[5,6]

$$\mathbf{P}_{\rm NL}(2\omega)=\chi^{(2),\rm SD}(2\omega;\omega,\omega):\mathbf{E}(\omega)\mathbf{E}(\omega)+\chi^{(2),\rm BQ}(2\omega;\omega,\omega):\mathbf{E}(\omega)\mathbf{E}(\omega)i\mathbf{k}, \qquad (1)$$

where the surface dipole (SD) and the bulk quadrupole (BQ) nonlinear polarizations are given by the third- and fourth-rank tensor nonlinear (ND) susceptibilities $\chi^{(2),\rm SD}$ and $\chi^{(2),\rm BQ}$, respectively, and $\mathbf{E}(\omega)$ and $\mathbf{k}$ are the amplitude and the wave vector of the pump radiation, respectively. Because for Si(111) the bulk quadrupole term $\mathbf{P}^{\rm BQ}$ cannot be distinguished from the surface dipole term $\mathbf{P}^{\rm SD}$ in experiment with a single fundamental beam, we will treat them together as an effective contribution $\mathbf{P}_{\rm NL}$. The external dc electric field applied to the crystal breaks its centrosymmetry and allows a bulk electric dipole contribution

$$\mathbf{P}^{\rm BD}(2\omega)=\chi^{(3)}(2\omega;\omega,\omega,0):\mathbf{E}(\omega)\mathbf{E}(\omega)\mathbf{E}_{\rm dc}, \qquad (2)$$

where $\mathbf{E}_{\rm dc}$ is the amplitude of the dc electric field. The nonzero components of $\chi^{(3)}$ in the crystallographic frame are presented in Table I. Note that for a crystal with point group O_h, like silicon, there are just three nonequivalent tensor components χ_1, χ_2, and χ_3. After transformation from the crystallographic to the interface frame, these components produce the effective nonlinear tensor component $\chi_{xxxz}=\sqrt{2}/6(\chi_1-2\chi_2-\chi_3)$. The interface frame xyz is chosen in such a way that $x\|\langle 11\bar{2}\rangle$, $y\langle\bar{1}10\rangle$, and $z\|\langle 111\rangle$, i.e., the z axis is the normal to the surface of the Si(111) crystal, and the xy plane coincides with the Si-SiO_2 interface. In the transmission geometry used in our experiments, only the susceptibility tensor component χ_{xxxz} produced the dc-induced nonlinear polarization $\mathbf{P}^{\rm BD}$. The total SHG intensity can then be written as

$$I_{2\omega}^{\rm trans}=|(L_{2\omega,\rm SD}\mathbf{P}^{\rm SD}+L_{2\omega,\rm BQ}\mathbf{P}^{\rm BQ}+L_{2\omega,\rm BD}\mathbf{P}^{\rm BD})L_\omega^2|^2, \quad (3)$$

where L_ω and $L_{2\omega}$ are the linear Fresnel factors at ω and 2ω, respectively. The latter can be different for the various contributions. In general, the nonlinear polarization vectors $\mathbf{P}^{\rm SD}$, $\mathbf{P}^{\rm BQ}$, and $\mathbf{P}^{\rm BD}$ will give rise to interference effects because of their complex nature, and the cross terms depend on the phase shifts between them.

For a MOS structure, due to the charge redistribution between the semiconductor and the metal, thermal equilibrium is established in such a way that the Fermi levels on both sides line up and a SCR is produced near the semiconductor surface[21] (Fig. 1). Therefore, even in the absence of an external field, there is an intrinsic dc electric field near the Si-SiO_2 interface and the bulk electric dipole source $\mathbf{P}^{\rm BD}$ by Eq. (2) is nonzero. The application of an external dc field affects the SCR and varies the value of $\mathbf{P}^{\rm BD}$. Note that although $\mathbf{P}^{\rm BD}$ is governed by a fourth-rank tensor $\chi^{(3)}$, the electric-field-induced SHG signal could be significant because of the considerable value of the electric field inside the SCR (near 10^5 V/cm) and the large thickness of the SCR. Here we assume that the external dc electric field, produced by the application of a bias voltage on the MOS structure, is oriented just along the surface normal z, and therefore we will use a one-dimensional approach. Since the dc electric field varies appreciably along the penetration depth of the SHG radiation $z_{2\omega}$, a more rigorous expression for $\mathbf{P}^{\rm BD}$ is the form

$$\mathbf{P}_{\rm eff}^{\rm BD}=\chi^{(3)}:\mathbf{E}(\omega)\mathbf{E}(\omega)\int\mathbf{E}_{\rm dc}(z)dz, \qquad (4)$$

where the integration is taken over $z_{2\omega}$ and the subscript eff denotes the fact that here we neglected retardation effects (see below).

Considering the SHG from Si-SiO_2 interfaces one should take into account the dependence of the SHG intensity on the silicon oxide thickness due to multiple reflections in the SiO_2 layer.[22,23] The SiO_2 layer also affects the electric field inside the Si through the voltage drop across it, as well as because of charges located at the Si-SiO_2 interface and/or trapped in the SiO_2 layer.

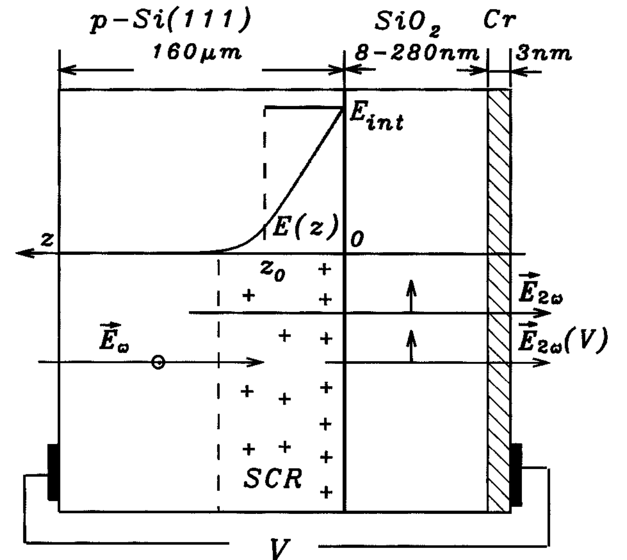

FIG. 1. The schematic diagram of the MOS structure studied.

III. EXPERIMENTAL METHODS

The schematic diagram of the MOS structure under investigation is presented in Fig. 1. The samples were p-type (5×10^{15} cm^{-3}, B doped) Si(111) ($\pm0.5°$) 0.16-mn wafers with both polished sides. A high-quality thermal oxide with a thickness of 300 nm was grown at the front side of the wafer at 1000 °C. To produce a smooth Si-SiO_2 interface, these samples were annealed at a slightly higher temperature in a nitrogen atmosphere. A buffered NH_4F-etch solution was used to etch the SiO_2 layer to prepare different oxide thicknesses ranging from 8 to 280 nm on a single Si substrate. High-resolution transmission electron microscopy images showed that the buried Si-SiO_2 interface was flat with a corrugation of two atomic layers over macroscopic distances (about 100 μm), and that the etching of SiO_2 did not influence the Si-SiO_2 interface. Single-wavelength ellipsometry with a HeNe laser was used to measure the SiO_2 thicknesses prior to and after etching. The front side semitransparent metal electrode was prepared by evaporating a chromium layer of ~3-nm thickness. A strip aluminum back electrode was evaporated near the edge of the wafer. Gold wires were attached to the electrodes by an In-Ga eutectic and silver paint. High-frequency C-V measurements were performed to characterize the prepared MOS structures.

For the SHG experiments we used the output at 1064 nm of a Q-switched Nd:YAG (yttrium aluminum garnet) laser. The laser generated 8-ns pulses at 10 Hz with 24-mJ energy in a 4.5-mm-diameter spot, well below the damage threshold. The SHG was studied in transmission, with the fundamental beam focused on the polished back side of the silicon wafer along their normal. The SHG signal was detected by a monochromator, photomultiplier, and gated electronics. The electric-field-induced effects in the SHG were measured in perpendicular polarization combination of fundamental and SHG radiation. The oxide thickness dependence was obtained by translating the sample through the laser beam, thereby keeping the same alignment.

IV. RESULTS AND DISCUSSION

A. Experimental results

We first measured the dependence of the SHG intensity on the silicon oxide thickness prior to and after the chromium evaporation, as recent experiments have shown a strong oxide thickness dependence of the SHG response due to multiple reflections for both ω and 2ω.[22] The model of multiple reflections is seen to describe the observed thickness dependences well. These results are used in the following calculations to normalize the SHG intensity for various oxide thicknesses. For the normal-incidence transmission geometry used in our experiments, a completely anisotropic SHG signal was measured, in agreement with theory.[5] The azimuthal rotational curves remained completely anisotropic for the applied biases,[18] as was expected from symmetry reasons. Thus all the bias dependences were measured at the maximum of the rotational anisotropy. A possible contribution from the Cr layer is expected to be isotropic, and can thus be neglected.

Figure 2 shows the dependences of the SHG intensity on the applied bias voltage for various oxide thicknesses. Parabolic dependences are observed near the minimum of the bias dependence, although deviations from this are seen for all but the thickest oxide. The minimum of the EISH bias dependences becomes sharper, and shifts toward lower bias voltages with decreasing oxide thickness.

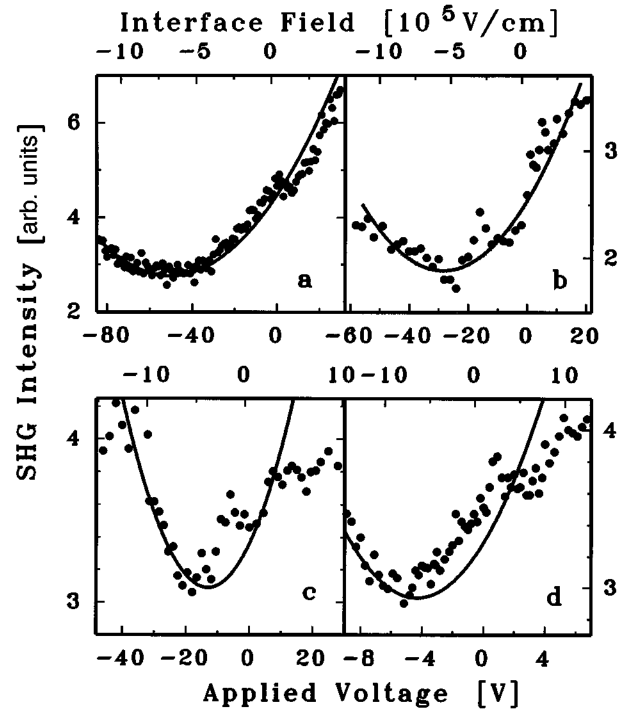

FIG. 2. The SHG intensities $I_{2\omega}$ vs an applied bias voltage V (lower axes) and an interface dc electric field $E_{\rm int}$ (upper axes) for MOS samples with various oxide thicknesses: (a) 234 nm, (b) 158 nm, (c) 101 nm, and (d) 18 nm. Measurements were performed in the maximum of the rotational anisotropic dependence. Solid lines present model parabolical curves obtained within the interface field approximation.

B. Interface electric-field approximation: Role of the oxide layer

The electric-field-induced nonlinear polarization $\mathbf{P}^{\rm BD}(z)$ is proportional to the electric field inside the SCR at position z. However, we will demonstrate here that most of the EISH features, such as the parabolical shape of the bias dependences and the linear dependence of their minima vs oxide thickness, can be described within a simple model, in which it is assumed that $\mathbf{P}^{\rm BD}$ is proportional to the electric field $E_{\rm int}\equiv E(z=+0)$ in the SCR just at the interface. This implies that the real field distribution $E_{\rm dc}(z)$ in the SCR is replaced by a constant $E_{\rm int}$ inside a layer of effective length z_0 that is comparable with the SCR width. z_0 should be chosen in such a way that $E_{\rm int}z_0(E_{\rm int})=\int E_{\rm dc}(z)dz$, where the integration over the SCR is such that it includes the charge conservation inside the SCR. We call this the interface field approximation. Since the experimental bias dependences were measured vs applied voltage, we should rescale the bias voltage units to the interface electric-field ones. To find the chromium electrode potential $\varphi(-L_d)$ with respect to the Si bulk (the latter is supposed to be neutral), one should solve the Poisson equation with the appropriate

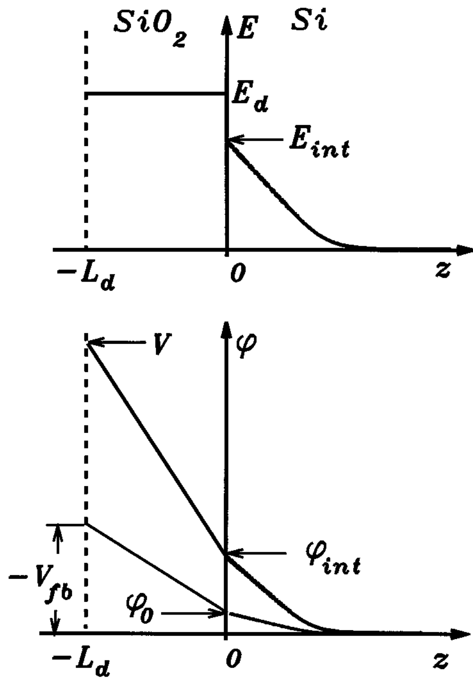

FIG. 3. The diagram of the potential and field distribution in Si and SiO_2.

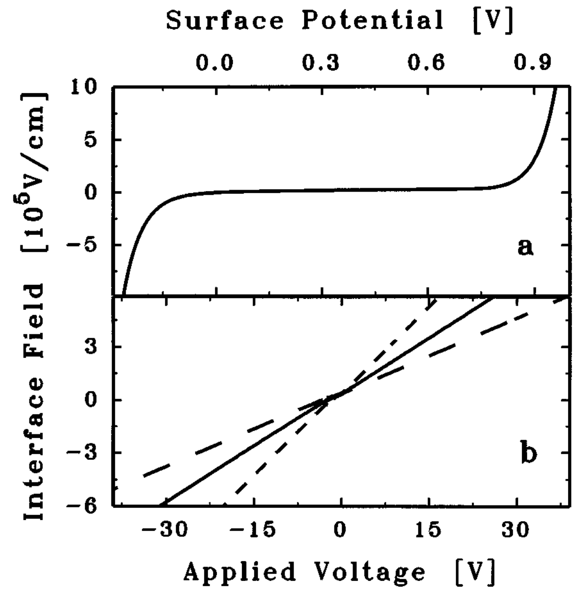

FIG. 4. The interface dc electric field E_{int} vs the interface potential φ_{int} [panel (a)] and an applied bias voltage V for various oxide thicknesses [panel (b)]: long dashed line, 234 nm; solid line, 158 nm; middle dashed line, 101 nm.

boundary conditions[24] in the one-dimensional geometry presented in Fig. 3, in the range of $-L_d<z<+\infty$. To do this, it is necessary to know the charge-density distribution $\rho(z)$ across the oxide layer. From C-V measurements, we have found that our samples have small densities of mobile charges and interface states D_{it} (below 10^{11} states eV^{-1} cm^{-2}) in comparison with the number of fixed charges that are distributed inside the SiO_2 layer up to 1 nm from the interface (the surface density $Q_f=5.5\times10^{11}$ traps cm^{-2}). The latter can easily be taken into account by the boundary condition at $z=0$, and we assume that

$$\rho(z)=0,\quad -L_d<z<-0,\quad \varepsilon_{\mathrm{sc}}E_{\mathrm{int}}-\varepsilon_d\mathbf{E}_d=4\pi Q_f,$$
$$\varphi(z=+\infty)=0, \tag{5}$$

where φ is the electrostatic potential, $\varepsilon=\varepsilon_{\mathrm{sc}}(\varepsilon_d)$ is the static dielectric constant for the semiconductor or the dielectric (SiO_2), respectively, L_d is the silicon oxide thickness, and $E_d\equiv E(z=-0)$ is the electric field inside the oxide. Thus the chromium potential consists of the potential of the Si-SiO_2 interface $\varphi_{\mathrm{int}}=\varphi(z=+0)$, and the voltage drop across the oxide layer:

$$\varphi(-L_d)=(\varepsilon_{\mathrm{sc}}E_{\mathrm{int}}-4\pi Q_f)L_d/\varepsilon_d+\varphi_{\mathrm{int}}, \tag{6}$$

where E_{int} as a function of φ_{int} can be derived as a first integral of the Poisson equation. To find the relationship between the external bias voltage V and the interface electric field E_{int} one should realize that even in the absence of an external bias voltage a SCR is produced. Due to the initial conditions $\varphi_{\mathrm{int}}=\varphi_0$ and $E_{\mathrm{int}}=E_0$, the expression for V has the form

$$V=(E_{\mathrm{int}}-E_0)\varepsilon_{\mathrm{sc}}L_d/\varepsilon_d+(\varphi_{\mathrm{int}}-\varphi_0). \tag{7}$$

Figure 4(a) presents the interface field E_{int} vs the interface potential φ_{int}, which was obtained by numerically solving the Poisson equation under the assumption that the local concentrations of holes $p(z)$ and electrons $n(z)$ are obeying Boltzmann statistics as long as in impunity concentration in the semiconductor is low enough to make the Fermi-Dirac ensemble nondegenerate. Using this and Eq. (7) we can easily find the E_{int} vs the applied bias V [Fig. 4(b)]. The resulting interface electric fields are plotted in Fig. 2, upper axes. For the oxide thicknesses used E_{int} depends almost linearly on the applied bias, and the EISH intensity should be quadratic in both the dc electric field and the bias, as is indeed observed in the data. Therefore, the thick oxide layer not only changes the bias voltage scale, but also changes the relationship between the *applied* bias and the electric field inside the SCR: instead of a strong nonlinear dependence $E_{\mathrm{int}}(\varphi_{\mathrm{int}})$, $E_{\mathrm{int}}(V)$ becomes quite linear. One can easily find the validity range of the interface field approximation—it is valid as long as the dependence $E_{\mathrm{int}}(V)$ remains linear. Note that this is in contradiction with previous works,[16,25–27] where it was assumed (explicitly or implicitly) that the potential drop *across the SCR* was proportional to the interface electric field. To fit the experimental data, a quadratic dependence of the SHG intensity on this drop was previously used, which is not very realistic considering the strong nonlinear behavior of E_{int} vs φ_{int}.

Within the interface field approximation, the minimum of the parabolic bias dependence should correspond to the flatband potential, i.e., the potential of the Si-SiO_2 interface with respect to the bulk silicon for which $E_{\mathrm{int}}=0$. In accordance with Eq. (7), the corresponding value of the external bias V_{fb} voltage is given, by

$$V_{\mathrm{fb}}=-E_0\varepsilon_{\mathrm{sc}}L_d/\varepsilon_d-\varphi_0. \tag{8}$$

which depends only on the initial band bending. The flatband voltage values were obtained from capacitance-voltage

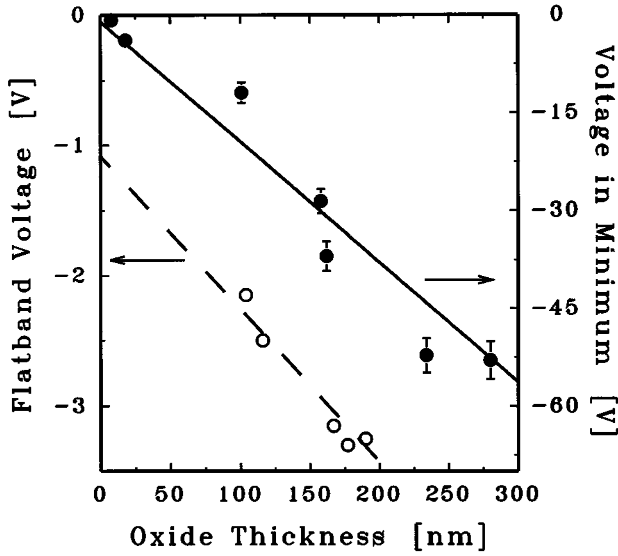

FIG. 5. Position of the minimum of bias dependence V_0 (right axis) and the flatband voltage V_{fb} (left axis) vs the oxide thickness L_d. Lines present the model curves.

(C-V) measurements using MOS structures prepared from an identical silicon wafer with an aluminum top electrode. The experimental data on V_{fb} vs silicon oxide thickness are presented in Fig. 5 (left axis). Following Eq. (8) this dependence was fitted by a linear function with E_0 and φ_0 as adjustable parameters. As a result, the value of the initial potential of the Si-SiO_2 interface is shown to be $\varphi_0=1.09$ V. To find the analogous values for the MOS structures studied, one should take into account the difference in work functions of aluminum and chromium $\Delta\phi=-0.33$ V.[21] In principle one could obtain the flatband position from the minimum of the voltage dependence of SHG. However, due to the interference between the various nonlinear contributions [Eq. (3)], the minima of the parabola are shifted away from the flatband voltage, and the voltage corresponding to the minimum of the EISH bias dependences becomes a linear function of the silicon oxide thickness:

$$V_0=(E_{\mathrm{int}}^{\mathrm{min}}-E_0)\varepsilon_{\mathrm{sc}}L_d/\varepsilon_d+(\varphi_{\mathrm{int}}^{\mathrm{min}}-\varphi_0), \tag{9}$$

where $\varphi_{\mathrm{int}}^{\mathrm{min}}$ is the electric potential of the Si-SiO_2 interface vs silicon bulk, and $E_{\mathrm{int}}^{\mathrm{min}}$ is the electric field in the minimum of the EISH curve. $\varphi_{\mathrm{int}}^{\mathrm{min}}$ and $E_{\mathrm{int}}^{\mathrm{min}}$ are expected to be oxide thickness independent. Equation (9) can be written in the form

$$V_0=E_{\mathrm{int}}^{\mathrm{min}}\varepsilon_{\mathrm{sc}}L_d/\varepsilon_d+\varphi_{\mathrm{int}}^{\mathrm{min}}+V_{\mathrm{fb}}, \tag{10}$$

where the flatband voltage V_{fb} is calculated from the C-V data for every silicon oxide thickness. The dependence $V_0(L_d)$ for all samples studied is depicted in Fig. 5 (right axis), and can be fitted by a linear function, showing a good agreement with the approach used.

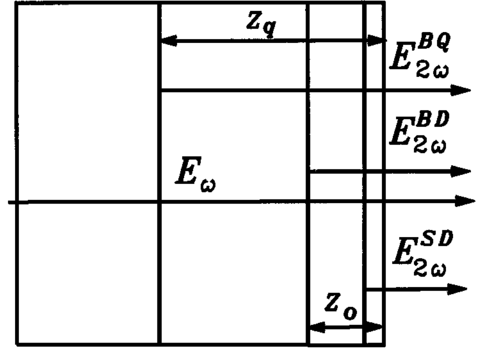

FIG. 6. The schematic diagram of the three-slab system used for consideration of retardation effects. Only Si is depicted.

C. Nonlinear interference in the EISH generation: Role of retardation effects

The interface field approximation is shown to describe the parabolical bias dependences observed for thick oxides very well. However, this model uses local phases of the various contributions to the polarization and neglects the phase differences that arise due to the spatial separation of the bulk nonlinear sources over distances, comparable with the second-harmonic wavelength. Including these retardation effects can significantly change the resulting SHG intensity, as can already be observed in Fig. 2.

Let us consider the model of the nonlinear source distribution as depicted in Fig. 6. There are three particular sources of the total SHG field. The first is the surface dipole source, localized in an interfacial region with a thickness d of a few atomic layers and contributing to the surface dipole polarization $\mathbf{P}^{\mathrm{SD}}$. Since $d\ll\lambda_{2\omega}$, where $\lambda_{2\omega}$ is the second-harmonic wavelength inside the silicon, one can use the approach of a thin nonlinear slab.[28,29] The bulk quadrupole source is spread out in a layer with an effective thickness of the penetration depth of the SHG field $z_{2\omega}$ and produces the bulk quadrupole contribution $\mathbf{P}^{\mathrm{BQ}}$. The thickness of this layer is bias independent, and the SHG radiation from quadrupole sources can effectively be described within a model of a thick (i.e., comparable with the second-harmonic wavelength) homogeneous nonlinear slab with the constant thickness z_q. Third, there are the bulk dipole sources. In the presence of a dc electric field, they give rise to the $\mathbf{P}^{\mathrm{BD}}$ nonlinear polarization and are localized in the SCR near the Si-SiO_2 interface. Within the frame of the interface field approximation they can be described by a thick homogeneous nonlinear slab with a *field-dependent thickness* $z_0(E_{\mathrm{int}})$. Note that for the transmission geometry used, there is no surface quadrupole SHG wave arising due the fundamental wave discontinuity at the interface.[29] The retardation effects will be significant if the relation between presented lengths is as follows:

$$d\ll z_0\sim z_q \tag{11}$$

For our samples (doping concentration $N_a\sim5\times10^{15}$ cm^{-3}) and the SH wavelength used (532 nm), we indeed have $z_0\leq0.5$ μm and $z_q\sim1$ μm.

To determine the total SHG field produced by these three slabs, one should solve the wave equation for the SHG field with the corresponding Green function. There are a number of works on such calculations for this problem.[30,31] However, due to the simplicity of our transmission geometry we will use the results of Ref. 28 and the following approach. First, in our experiment $\mathbf{P}^{BQ}$ cannot be separated from $\mathbf{P}^{SD}$, and therefore we have used an effective polarization $\mathbf{P}_{NL}$ that includes $\mathbf{P}^{BQ}$ and $\mathbf{P}^{SD}$. Second, we will consider the EISH wave $\mathbf{E}^{BD}(2\omega)$, which is generated by $\mathbf{P}^{BD}$, and the field-independent SHG wave $\mathbf{E}^{S,B}(2\omega)=\mathbf{E}^{BQ}(2\omega)+\mathbf{E}^{SD}(2\omega)$ separately. According to Ref. 28 we obtain an expression for $\mathbf{E}^{BD}(2\omega)$ at the interface in the form

$$\mathbf{E}^{BD}(2\omega,z=-0)-\alpha\mathbf{P}^{BD}[-1+\exp(i\gamma z_0(E_{int}))], \quad (12)$$

with

$$\alpha=4\pi[(\sqrt{\varepsilon}+\sqrt{\varepsilon_T})(\sqrt{\varepsilon_S}-\sqrt{\varepsilon})]^{-1},$$

$$\gamma=2(\sqrt{\varepsilon_S}-\sqrt{\varepsilon})\omega/\mathbf{c}, \quad (13)$$

where ε_S and ε denote the dielectric constants of silicon at ω and 2ω, respectively, and ε_T that of SiO_2 at 2ω. Equation (12) contains the boundary SHG wave created at $z=z_0$ and the dipole-amplified (i.e., amplified by the bulk dipole sources) EISH wave. Here for the sake of simplicity we neglect the nonlinear polarization, produced by the fundamental wave, reflected from the Si-SiO_2 interface; however, it can easily be taken into account in more rigorous approach. The amplitude of $\mathbf{E}^{S,B}(2\omega)$ at the interface can be given effectively by

$$\mathbf{E}^{S,B}(2\omega,z=-0)=\mathbf{B}+i\mathbf{C}. \quad (14)$$

Here

$$\mathbf{B}=\alpha\mathbf{P}^{BQ}\sin(\gamma z_q),$$

$$\mathbf{C}=\alpha\mathbf{P}^{BQ}[-1+\cos(\gamma z_q)]+\mu\mathbf{P}^{SD}, \quad (15)$$

$$\mu=8\pi\omega d[c(\sqrt{\varepsilon}+\sqrt{\varepsilon_T})]^{-1},$$

where we took account of the fact that the gradient operation in $\mathbf{P}^{BQ}$ produced a 90° phase shift. The total SHG wave at the interface is a simple superposition of these two fields $\mathbf{E}^{BD}$ and $\mathbf{E}^{S,B}$.

Now using Eq. (3) we can calculate the resulting SHG intensity, properly taking into consideration the nonlinear interference. For the x components of the SHG waves and nonlinear polarizations that are relevant in our geometry, we can write $\alpha\mathbf{P}_x^{BQ}=A$, and $E_x^{S,B}=B+iC$. For the total outgoing SHG intensity this yields

$$I_{2\omega}=|A[-1+\exp(i\gamma z_0)]+B+iC|^2. \quad (16)$$

Here only A and z_0 depend on the dc electric field inside the SCR. Within the interface field approximation we assume that $A=\alpha\chi^{(3)}E_{int}(L_\omega E_\omega)^2$. The cross terms with $A\exp(i\gamma z_0)$ will give rise to an oscillatoric behavior as a function of z_0, and thus of V. Although the dependence of z_0 vs E_{int} should be chosen in such a way that $E_{int}z_0(E_{int})=\int E_{dc}(z)dz$, for some region of the interface fields we can put $z_0=vE_{int}$ (this is true at least within the validity of the Schottky approximation[21]). Under these assumptions the dependence of the EISH intensity on E_{int} (and thus on the applied voltage V) should be a superposition of a parabola, an oscillatoric function with field-dependent amplitude and period, and a field-independent background. We fitted our experimental bias dependences by Eq. (16) with A, B, C, and v as adjustable parameters, and with the dielectric constants of Si from Ref. 32. The model curves are presented in Fig. 7, solid lines, and demonstrate an acceptable agreement with the experimental data.

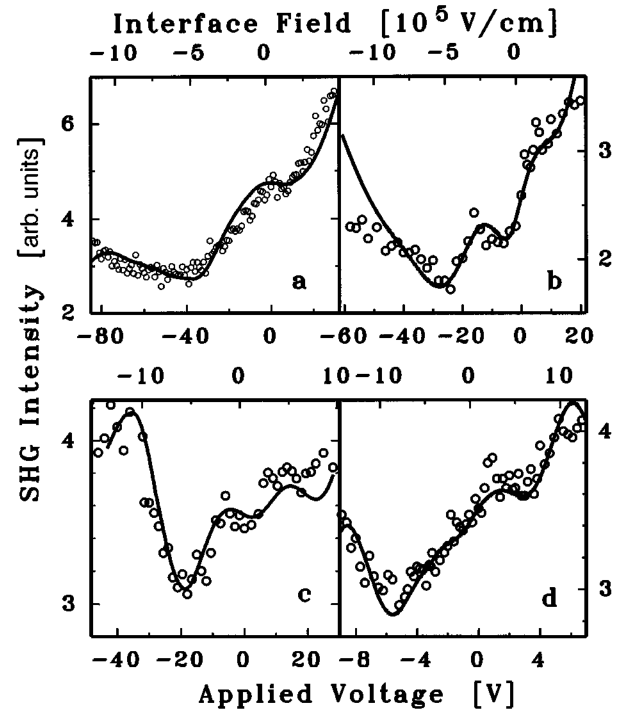

FIG. 7. The results of the fitting the experimental data, taking into account retardation of the EISH wave within the two-layer model for MOS samples with various oxide thicknesses: (a) 234 nm, (b) 158 nm, (c) 101 nm, and (d) 18 nm.

D. Influence of the dc-field spatial distribution inside the silicon on the EISH generation

Though the two-slab model presented in Sec. IV C describes the bias dependences for various oxides in the central range of interface fields quite well, one can hardly expect a good agreement between this approach and the experimental data for larger fields because of at least three factors. First, we considered retardation effects in the *homogeneous* nonlinear slabs. This implies that the amplitudes of the nonlinear polarizations remain constant along the slab. However, the dc electric field inside the SCR is strongly inhomogeneous, and gives rise to a dependence of a $\mathbf{P}^{BD}$ vs z. Second, the thickness of the dc-induced bulk dipole slab z_0 is supposed to be proportional to the interface field. This is hardly valid for strong inversion and accumulation regimes. Third, we neglected the absorption of the fundamental and the SHG waves inside the dc-induced slab, which can produce an additional retardation of the EISH wave. Actually, clear devia-

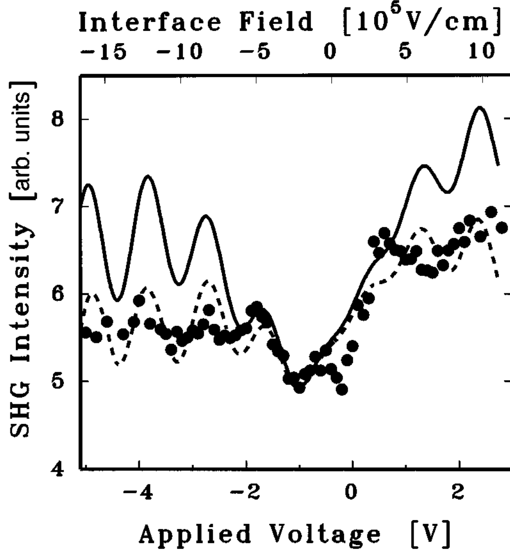

FIG. 8. The SHG intensity $I_{2\omega}$ vs an applied bias voltage V (lower axis) and interface dc electric field $E_{\rm int}$ (upper axis) for a MOS sample with the oxide thickness of 8 nm. The solid line is the best fit by the three-layered model. The dashed line presents the same curve, taking into consideration the dc-field spatial distribution.

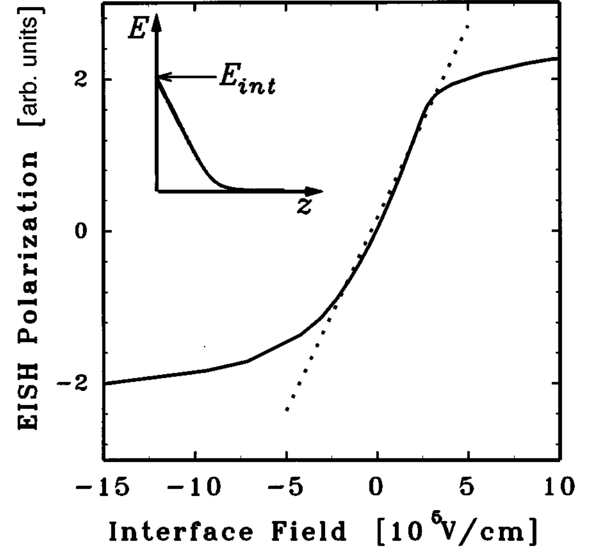

FIG. 9. The amplitude of the effective dc-induced nonlinear polarization $\mathbf{P}^{\rm BD}$, calculated by the integration Eq. (4) vs the interface dc-field strength $E_{\rm int}$ (solid line). The dot line presents the fit by the linear function of the central region. Inset: the scheme of the dc-field spatial distribution.

tions from the model were observed for the sample with an 8-nm-thick oxide, where larger fields were reached due to the thin oxide. Figure 8 shows the bias dependence for such a MOS structure, and the solid line presents the curve, obtained from Eq. (16). The model curve matches the experimental data well enough in the central voltage region, but starts to deviate for larger biases. Notice the trend in the bias dependence: pronounced oscillations are observed on a saturating background.

To try to understand the origin of this saturation and to assess the aforementioned reasons for the discrepancy between the model and the experiment as well, we will take into account the spatial distribution of the dc electric field inside the SCR, using the following approach. We will first numerically calculate the effective dc-induced polarization $\mathbf{P}_{\rm eff}^{\rm BD}$ by Eq. (4) (see the inset in Fig. 9). Then we will consider the two-layered system with a homogeneous bulk dipole slab, which gives rise to this nonlinear polarization. To evaluate $\mathbf{P}_{\rm eff}^{\rm BD}$ we use the first integral of the Poisson equation,

$$E^2(\varphi)=8\pi kT/\varepsilon_{\rm sc}\{p_0[\exp(-\xi\varphi)+\xi\varphi-1] + n_0[\exp(\xi\varphi)-\xi\varphi-1]\}, \quad (17)$$

where $\xi=e/(kT)$, and $p_0(n_0)$ are the equilibrium concentrations of the holes (electrons). Figure 9 presents the value of the $\mathbf{P}_{\rm eff}^{\rm BD}$ value as a function of the interface field. Notice the following general trend: the dc-induced nonlinear polarization saturates with the increasing absolute value of the interface field. Inside the corresponding field regions the dc-induced term in the nonlinear polarization becomes practically field independent, which obviously causes the saturation of the EISH signal. The calculated bias dependence in the two-slab system with the polarization of the bulk dipole slab $\mathbf{P}_{\rm eff}^{\rm BD}$ is presented in Fig. 8, dashed line, and is in good agreement with the experimental data. This indicates that the spatial distribution plays a key role in the deviations of the experimental points from the simple two-layer model. Notice that within a certain field region the dependence of $\mathbf{P}^{\rm BD}$ vs $E_{\rm int}$ can effectively be fitted by a linear function (dotted line in Fig. 9). This field region defines the frame of the validity of the interface field approximation.

Although for a rigorous analysis of EISH curves under strong inversion and accumulation conditions, one should take into account the deviation of the carrier statistics from the Boltzmann assembly, these calculations demonstrate the importance of the inclusion of the dc-electric-field distribution inside the SCR for a proper analysis of the EISH generation.

V. CONCLUSIONS

We have shown that the SHG from the Si(111)-SiO_2 buried interface significantly varies under the application of a dc electric field. The paraboliclike bias dependences of EISH, which have minima shifted away from zero voltage, indicate the presence of a considerable field-induced contribution to the nonlinear polarization even in the absence of an external bias. This bulk contribution can even dominate the SHG signal from unbiased Si(001)-SiO_2 interface, as was demonstrated recently in Ref. 19.

The interface field approximation was used to explain the parabolic shape of the bias dependences, and the role of the oxide thickness in this approach was discussed. The proper consideration of the EISH wave retardation was shown to be important for the explanation of the fine structure of the bias dependences. The nonlinear interference between field-dependent and independent contributions to the nonlinear polarization was taken into account. We have demonstrated the

role of the field distribution inside the space-charge region of silicon for a description of the dc-induced effects in SHG for larger voltages. However, it is worth noting that the retardation effects in the two-slab model of EISH are still incomplete, and a more rigorous phenomenological description is in progress.

The observed oxide-thickness dependence of EISH is completely described by the redistribution of the bias voltage across the MOS structure due to the voltage drop inside the SiO_2 film and multiple reflections inside the silicon oxide layer. Note that since EISH is generated by the dc electric field within the laser beam spot, it can be used as a local probe of variations in the charge distribution at the Si-SiO_2 interface.

ACKNOWLEDGMENTS

We are pleased to acknowledge stimulating discussions with L. V. Keldysh, I. M. Baranova, M. C. Downer, T. F. Heinz, J. I. Dadap, and J. Lowell. We would like to thank A. Nevzorov for *C-V* measurements, S. Bakker for preparation of the thick thermal oxide, and R. Gelsing for preparation of the Cr electrodes. This work was supported by the Russian Foundation of Basic Research (RFFI) Grant No. 95-02-05893a, INTAS-93 Grant No. 370, ISF Grant No. M12300, ''Physics of Solid State Nanostructures'' Program, and the Stichting voor Fundamental Onderzoek der Materie (FOM), which is financially supported by the Nederlandse Organisatie voor Wetenschappelijk Onderzoek (NWO).

[*]Author to whom correspondence should be addressed. Electronic address: aktsip@astra.phys.msu.su

[1]T. F. Heinz, in *Nonlinear Surface Electromagnetic Phenomena*, edited by H.-E. Ponath and G. I. Stegeman (North-Holland, Amsterdam, 1991), p. 355.

[2]J. F. McGilp, Prog. Surf. Sci. **49**, 1 (1995); G. L. Richmond, J. M. Robinson, and V. L. Shannon, *ibid.* **28**, 1 (1988).

[3]Th. Rasing, Appl. Phys. A **59**, 531 (1994).

[4]H. W. K. Tom, T. F. Heinz, and Y. R. Shen, Phys. Rev. Lett. **51**, 1983 (1983).

[5]O. A. Aktsipetrov, I. M. Baranova, and Yu. A. Ilinskii, Zh. Éksp. Teor. Fiz. **91**, 287 (1986) [Sov. Phys. JETP **64**, 167 (1986)].

[6]J. E. Sipe, D. J. Moss, and H. M. van Driel, Phys. Rev. B **35**, 1129 (1987).

[7]C. W. van Hasselt, M. A. Verheijen, and Th. Rasing, Phys. Rev. B **42**, 9263 (1990).

[8]G. G. Milliaras, H. A. Wierenga, and Th. Rasing, Surf. Sci. **287/288**, 703 (1993).

[9]G. Lupke, D. J. Bottomley, and H. M. van Driel, Phys. Rev. B **47**, 10 389 (1993).

[10]W. Daum, H.-J. Krause, U. Reichel, and H. Ibach, Phys. Rev. Lett. **71**, 1234 (1993).

[11]C. Meyer, G. Lupke, U. Emmerichs, F. Wolter, H. Kurz, C. H. Bjorkman, and G. Lucovsky, Phys. Rev. Lett. **74**, 3001 (1995).

[12]C. H. Bjorkman, C. E. Shearon, Y. Ma, T. Yasuda, G. Lucovsky, U. Emmerichs, C. Meyer, K. Leo, and H. Kurz, J. Vac. Sci. Technol. B **11**, 1521 (1993).

[13]J. I. Dadap, B. Doris, Q. Deng, M. C. Downer, J. K. Lowell, and A. C. Diebold, Appl. Phys. Lett. **64**, 2139 (1994).

[14]C. H. Lee, R. K. Chang, and N. Bloembergen, Phys. Rev. Lett. **18**, 167 (1967).

[15]O. A. Aktsipetrov and E. D. Mishina, Dokl. Akad. Nauk SSSR **274**, 62 (1984) [Sov. Phys. Dokl. **29**, 37 (1984)].

[16]O. A. Aktsipetrov, I. M. Baranova, L. V. Grigor'eva, K. N. Evtyukhov, E. D. Mishina, T. V. Murzina, and I. V. Chernyi, Kvant. Electron. (Moscow) **18**, 943 (1991) [Sov. J. Quantum Electron. **21**, 854 (1991)].

[17]O. A. Aktsipetrov, I. M. Baranova, K. N. Evtyukhov, T. V. Murzina, and I. V. Chernyi, Kvant. Electron. (Moscow) **19**, 869 (1992) [Sov. J. Quantum Electron. **22**, 807 (1992)].

[18]O. A. Aktsipetrov, A. A. Fedyanin, V. N. Golovkina, and T. V. Murzina, Opt. Lett. **19**, 1450 (1994).

[19]J. I. Dadap, X. F. Hu, M. H. Anderson, M. C. Downer, J. K. Lowell, and O. A. Aktsipetrov, Phys. Rev. B **53**, R7607 (1996).

[20]P. Godefroy, W. de Jong, C. W. van Hasselt, M. A. C. Devillers, and Th. Rasing, Appl. Phys. Lett. **68**, 1981 (1996).

[21]S. M. Sze, *Physics of Semiconductor Devices* (Wiley, New York, 1981).

[22]C. W. van Hasselt, M. A. C. Devillers, Th. Rasing, and O. A. Aktsipetrov, J. Opt. Soc. Am. B **12**, 33 (1995).

[23]C. W. van Hasselt, E. Mateman, M. A. C. Devillers, Th. Rasing, A. A. Fedyanin, E. D. Mishina, O. A. Aktsipetrov, and J. C. Jans, Surf. Sci. **331-333**, 1367 (1995).

[24]C. G. B. Garrett and W. H. Brattain, Phys. Rev. **99**, 376 (1955).

[25]P. R. Fischer, J. L. Daschbach, D. E. Gragson, and G. L. Richmond, J. Vac. Sci. Technol. A **12**, 2617 (1994).

[26]P. R. Fischer, J. L. Daschbach, and G. L. Richmond, Chem. Phys. Lett. **218**, 200 (1994).

[27]J. L. Daschbach, P. R. Fischer, D. E. Gragson, D. Demarest, and G. L. Richmond, J. Phys. Chem. **99**, 3240 (1995).

[28]N. Bloembergen and P. S. Pershan, Phys. Rev. **128**, 606 (1962).

[29]P. Guyot-Sionnest, W. Chen, and Y. R. Shen, Phys. Rev. B **33**, 8254 (1986).

[30]P. D. Maker, R. W. Terhune, M. Nisenoff, and C. M. Savage, Phys. Rev. Lett. **8**, 21 (1962); J. Jerphagnon and S. K. Kurtz, J. Appl. Phys. **41**, 1667 (1970).

[31]M. S. Yeganeh, J. Qi, J. P. Culver, A. G. Yodh, and M. C. Tamargo, Phys. Rev. B **46**, 1603 (1992); H. Wierenga, M. W. J. Prins, and Th. Rasing, Physica B **204**, 281 (1995).

[32]D. E. Aspnes and A. A. Studna, Phys. Rev. B **27**, 985 (1983).